05

Target expansion modelling for problems of laser ion acceleration optimization

© M.A. Rakitina[1], A.V. Brantov[1], S.I. Glazyrin[1,2]

[1] Lebedev Physical Institute, Russian Academy of Sciences,
119991 Moscow, Russia
[2] All-Russian Research Institute of Automation named after N.L. Dukhov,
127030 Moscow, Russia

e-mail: rakitinama@lebedev.ru

Received December 01, 2022
Revised January 09, 2023
Accepted January 28, 2023

At present, a significant part of experiments on the interaction of high-power short laser pulses with solid targets is faced with the problem of target modification under the action of a nanosecond prepulse. In this paper, a series of hydrodynamic calculations of target irradiation with a nanosecond laser pulse is performed, which describes the plasma density profiles arising during the target expansion as a function of the parameters of the laser prepulse/additional pulse. The results obtained can make it possible to improve the efficiency of ion acceleration in the interaction of short laser pulses with a profiled plasma target.

Keywords: preplasma, laser-plasma interaction, plasma expansion, laser ion acceleration.

DOI: 10.61011/EOS.2023.02.55782.20-23

1. Introduction

Experiments on the generation of beams of high-energy ions during the interaction of laser pulses with various targets are of considerable interest due to the possibility of their practical applications for diagnostic purposes, creation and study of matter in extreme states, initiation of nuclear reactions to obtain medical isotopes and neutrons [1,2]. The laser pulse irradiates the target, usually a thin foil, accelerating the electrons near the frontal surface of the target to relativistic velocities. A large fraction of the accelerated electrons passes through the target and creates an electrostatic charge separation field that accelerates ions from the rear surface of the target. In the described scheme (called TNSA [1,2] in the English-language sources), the efficiency of electron heating, which is largely determined by the characteristics of the pre-plasma arising on the front surface of the target, also determines the ion acceleration efficiency [3–8].

The plasma profile at the target front can arise due to the existence of a pre-pulse associated with the final contrast of a short femtosecond laser pulse [6], as well as created specifically by exposure to an additional, usually nanosecond pulse synchronized with the main pulse [4]. It was predicted that fairly sharp density gradients near its critical value (on the order of $4-6\,\mu$m) are optimal for ion acceleration [4,5,7,8]. Note that the presence of a pre-plasma leads to a change in the optimal target thickness for ion acceleration [3], which may be due to the destruction of the back side of the target, leading to a decrease in the energy of the accelerated ions [9]. It is also possible to control the direction of the accelerated proton beam by adjusting the pre-pulse, as shown in [6].

Thus, controlling the target's expansion and creating a pre-plasma with a high density gradient on the irradiated side (on the order of $4-6\,\mu$m) can significantly increase the efficiency of laser ion acceleration if it is possible to avoid destroying the back side of the target. In this work, a series of hydrodynamic calculations were carried out, showing the dependence of the pre-plasma profile of the dispensing target on the energy density of the irradiating nanosecond laser pulses and predicting the possibility of obtaining optimal density gradients.

2. Problem formulation

The purpose of the calculations — to study the plasma density profile when irradiating the target with a laser pulse of nanosecond duration. The calculations used laser pulses with intensities from 10^8 to 10^{13} W/cm^2, duration from 1 to 5 ns (half-width of the time Gaussian envelope of the pulse, maximum arrival time $t_0 = 10$ ns) and focus radius from 3 to 18 μm (characteristic radius in the transverse Gaussian intensity distribution). The target has a flat geometry and is filled with a homogeneous substance with normal density ρ_0 (for aluminum, $\rho_0 = 2.7$ g/sm^3). The laser pulse falls along the normal to the surface, which causes it to heat up, evaporate, and fly off into a vacuum. The Euler-type hydrodynamic code used in the numerical simulation (details of the physical models implemented in the code are described below) does not allow us to describe the vacuum state directly, so a low-density medium (for simplification with the same equation of state as the target

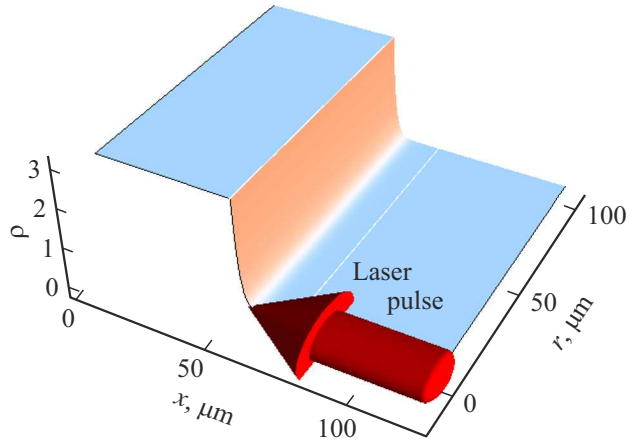

Figure 1. Modelling details. The surface shows the density value $\rho(r, x)$. The laser pulse falls in the direction of the X axis, as marked by the red arrow, and has a Gaussian profile along the radius.

substance) is specified instead of vacuum. At sufficiently low density ρ_1, such an environment has no effect on the expansion dynamics of the target itself, which is directly verified by further decreasing the environment density: the result is independent of their density. In the calculations below, the value $\rho_1 = 2 \cdot 10^{-5}\rho_0$ was used. Another formulation modification, related to the requirement of numerical algorithms: the transition between the target and the surrounding low-density matter must be smooth, so in the transition area the density is set varying by exponent. At $x > x_0$

$$\rho(x) = \rho_1 + (\rho_0 - \rho_1)\exp\big(-(x - x_0)/\delta\big),$$

where $x_0 = 50\,\mu$m — position of the target boundary, $\delta = (0.5{-}1)\,\mu$m —- small transition thickness. It is important to ensure that the size of the transition area δ is much smaller than the further scale of plasma expansion, in this case, the forming plasma corona does not depend on δ, which is also clearly verified in the calculations. The initial target temperature was set at 0.01 eV, at which the pressure in the target is negligibly small compared to the pressure in the laser absorption area. The initial formulation is chosen so that additional parameters, other than the target substance and its initial density, have no influence on the further dynamics of target expansion. The scheme of the problem formulation is shown in Figure 1.

The simulation was performed using the FRONT hydrodynamic code, which solved a system of two-temperature hydrodynamic equations [10]. The heat flux was calculated by Spitzer–Harm using the heat transfer limiting constant (in our calculations 0.15), and ionization — with the Saha equilibrium ionization model. The intensity equation was solved together with the hydrodynamic equations, i. e., at each numerical time step the intensity equation was integrated along the beam with the current density and temperature profiles. The absorption coefficient k was determined by the inverse-braking mechanism. Most of the calculations were done for the aluminum target. Titanium and carbon targets were also used. The calculations were performed in three-dimensional (in rx-cylindrical geometry with angular symmetry).

3. Results of the target expansion

Fig. 2 shows the plasma density profiles during the arrival of a maximum laser pulse with energies of (a, b) and 0.05 mJ (c, d) on the aluminum target and 5 ns duration, the pulse is focused into a hot spot with a radius of 10 (a, c) and $5\,\mu$m (b, d). Fig. 2 shows that as the laser pulse energy increases, the differences in the density profiles become less visible, as long as the input energy is the same.

At intensities of $I > 10^{11}$ W/cm^2 for $\tau = 5$ ns, shock waves running inside the target lead to a significant densification of the plasma density profile (a peak area appears) and shift the dense layers of the target inward. Thus, if at an energy density of $\sim 10^2$ J/cm^2 the aluminum target shifts inward by $5\,\mu$m (Fig. 2, d), then at an energy density of $\sim 10^4$ J/cm^2, the shift reaches $20\,\mu$m (Fig. 2, b). It is also worth noting that the characteristic gradients are preserved when displaced from the center by up to $7\,\mu$m in the transverse direction at a focus spot of $10\,\mu$m.

The longitudinal plasma density profiles obtained in hydrodynamic simulations can be described using two exponents with characteristic gradients in the following form (in center of the laser beam, $r = 0$):

$$n(x) = n_1\theta(x_c - x)\exp(-x/L_1) + n_0\theta(x - x_c) \times \exp\big(-(x - x_c)/L_0\big).$$

This approximation, although rather crude, is the most convenient for further modeling and allows to describe the behavior of the plasma density profile in the near-critical area and in the area of low-density plasma. Here, the point corresponding to the transition between the two characteristic gradients, x_c, corresponds to a density coordinate varying from $0.3n_c$ to $0.1n_c$ as the momentum intensity increases, n_c — critical density.

The characteristic gradients (Fig. 3) are calculated in two cases — at the moment of complete passage of the laser pulse (shown in blue), which corresponds to the problem formulation using an additional laser pulse, and at the moment of arrival of the maximum intensity (shown in red), which corresponds to the problem formulation with the pre-pulse. Fig. 3 shows that for near-critical plasma, the growth rate of the characteristic gradient at the moment of the arrival of the intensity maximum slows down with increasing input energy. For a low-density pre-critical plasma, it can be seen that the characteristic density gradient continues to increase with increasing input energy, but becomes less dependent on the duration and intensity of the laser pulse for the same energy density values.

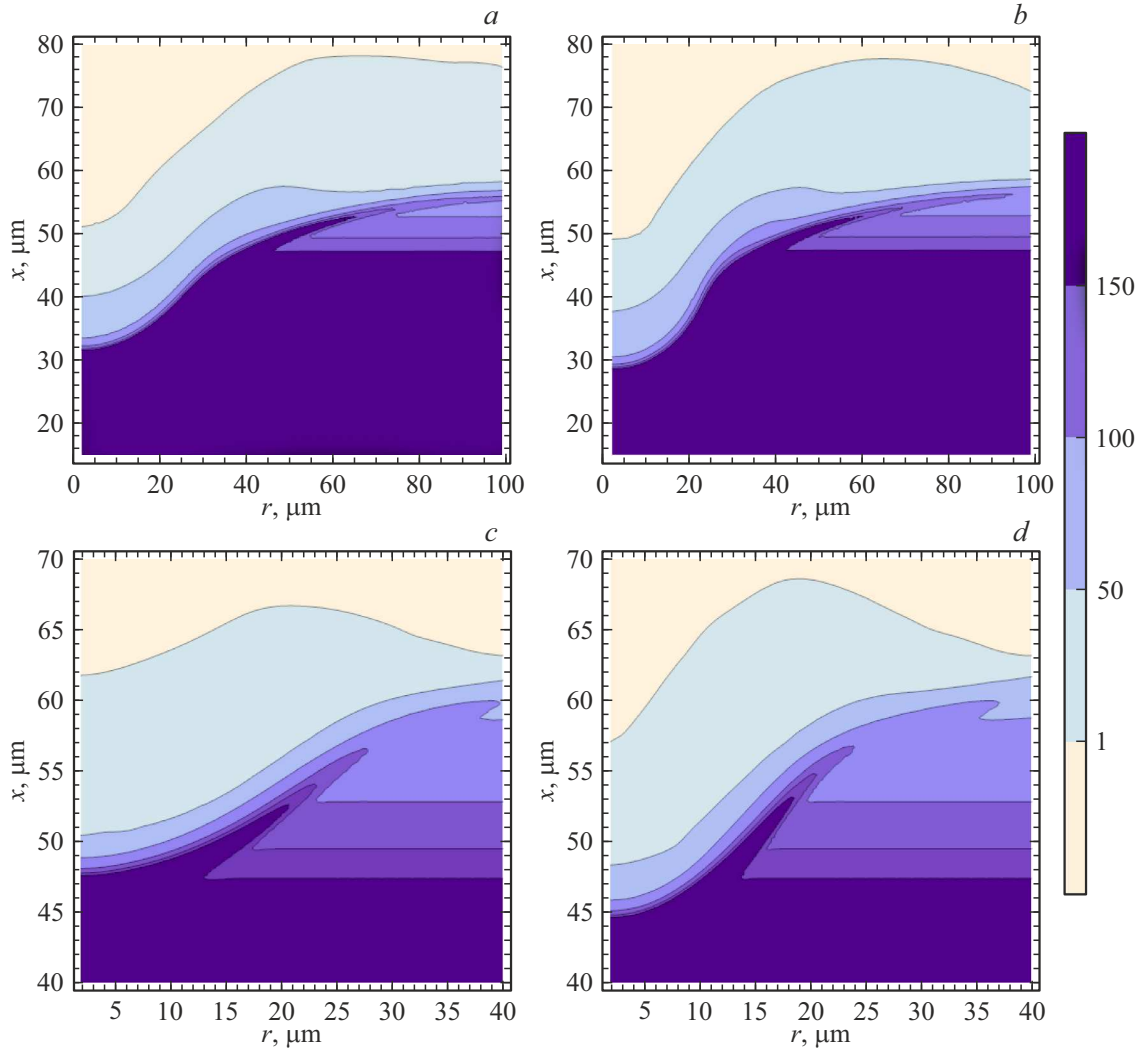

Figure 2. Plasma electron density profiles, n/n_c, obtained by irradiating an aluminum target with a 5 ns laser pulse with energy 5 (a, b) and energy 0. 05 mJ (c, d) at a focus spot of 10 (a, c) and 5 μm (b, d) at time 10 ns (when the maximum pulse arrives at the target).

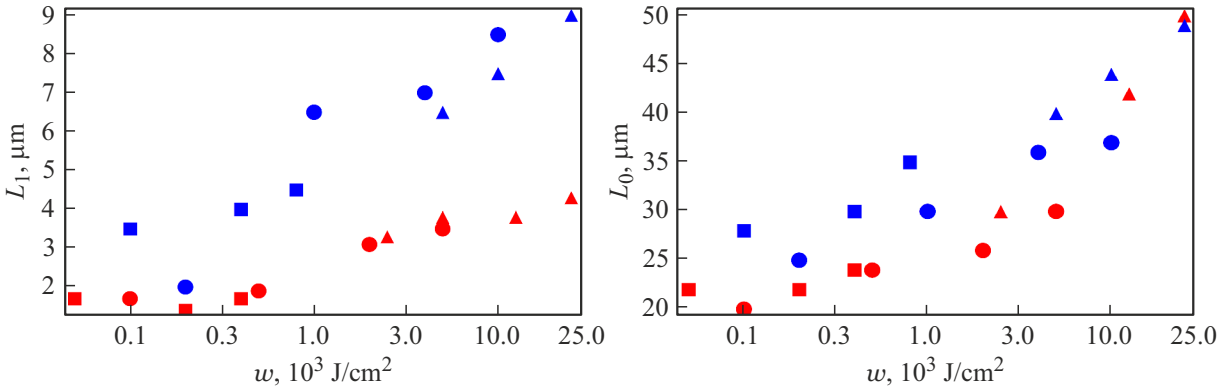

Figure 3. Dependence of the plasma density gradient (obtained from the formula for the approximate description) on the energy density w of the laser pulse near the critical density (L_1, left panel) and for the pre-critical low-density plasma (L_0, right panel) at the arrival of the pulse maximum (shown in red) and after the pulse has completely passed (shown in blue) at pulse durations 5 (squares), 3 (triangles), and 2 ns (circles).

The dependence of plasma density on target material, initial density profile, laser pulse duration and intensity at different energy densities were also studied. Carbon, titanium, and aluminum targets were considered, with energy densities varying from 10^2 to 10^5 J/cm^2. It is calculated that, for the considered parameters of laser pulses at energy densities exceeding 10^4 J/cm^2, the density profiles of the expanded plasma near the critical density practically do not depend on the initial density profile, intensity and duration of the pulse at the same values of its energy. Also, the plasma density profile is weakly dependent on the target material due to fast ionization. For energy densities lower than the threshold, the carbon target is stronger, and the titanium target is somewhat weaker than the aluminum one.

4. Conclusion

Studies have shown that at intensities exceeding 10^{10} W/cm^2 and energy densities above 10^4 J/cm^2, the profile of the expanded plasma near the critical density is determined mainly by the value of the input energy density. The characteristic plasma density profile gradients increase with growing laser energy density, while the rise of characteristic near-critical plasma gradients slows down at sufficiently high energy densities ($\sim 10^4$ J/cm^2). It is the energy density $\sim 3 \cdot 10^3 - 10^4$ J/cm^2 that allows the gradient around the critical density at $(4-6)\,\mu$m, which is optimal for ion acceleration [7,8]. In this case, the delay of the powerful femtosecond pulse should not exceed 3–5 ns after the arrival of the nanosecond pulse on the target as long as the gradient retains the necessary value. We should use targets with thicknesses on the order of $10-20\,\mu$m, the back side of which will not be destroyed at a given energy density, despite target shift [11]. Here, it is worth noting that further increasing the invested energy leads to the need to use thicker targets to avoid destroying them, which reduces the efficiency of femtosecond ion acceleration [1,2] pulses. Thus, the obtained plasma density profiles can be further used to optimize proton acceleration by a powerful femtosecond laser pulse, for example, to create a compact neutron source.

Funding

This study was carried out with the partial support of the Federal Scientific and Technical Program for the Development of Synchrotron and Neutron Research and Research Infrastructure for 2019–2027, dated 29.09.2021 № 2021-951-FP5-3, Agreement № 075-15-2021-1361 dated 07.10.2021 with Ministry of Education and Science of Russia.

Conflict of interest

The authors declare that they have no conflict of interest.

References

[1] H. Daido, M. Nishiuchi, A. S. Pirozhkov. Rep. Prog. Phys., **75** (5), 056401 (2012). DOI: 10.1088/0034-4885/75/5/056401
[2] A. Macchi, M. Borghesi, M. Passoni. Rev. Mod. Phys., **85** (2), 751 (2013). DOI: 10.1103/RevModPhys.85.751
[3] M. Kaluza, J. Schreiber, M.I.K. Santala, G.D. Tsakiris, K. Eidmann, J. Meyer-ter-Vehn, K.J. Witte. Phys. Rev. Lett., **93** (4), 045003-1 (2004). DOI: 10.1103/PhysRevLett.93.045003
[4] P. McKenna, D.C. Carroll, O. Lundh, F. Nürnberg, K. Markey, S. Bandyopadhyay, D. Batani, R.G. Evans, R. Jafer, S. Kar, D. Neely, D. Pepler, M.N. Quinn, R. Redaelli, M. Roth, C.-G. Wahlström, X.H. Yuan, M. Zepf. Laser and Particle Beams, **26** (4), 591 (2008). DOI: 10.1017/S0263034608000657
[5] A. Yogoa, H. Daido, A. Fukumi, Z. Li, K. Ogura, A. Sagisaka, A.S. Pirozhkov. Phys. Plasmas., **14** (4), 043104 (2007). DOI: 10.1063/1.2721066
[6] A. Yogo, H. Kiriyama, M. Mori, T.Zh. Esirkepov, K. Ogura, A. Sagisaka, S. Orimo, M. Nishiuchi, A.S. Pirozhkov, H. Nagatomo, Y. Nakai, T. Shimomura, M. Tanoue, A. Akutsu, H. Okada, T. Motomura, S. Kondo, S. Kanazawa, S.V. Bulanov, P.R. Bolton, H. Daido. Eur. Phys. J. D., **55**, 421 (2009). DOI: 10.1140/epjd/e2009-00045-5
[7] L.A. Gizzi, E. Boella, L. Labate, F. Baffigi, P.J. Bilbao, F. Brandi, G. Cristoforetti, A. Fazzi, L. Fulgentini, D. Giove, P. Koester, Da. Palla, P. Tomassini. Sci Rep., **11**, 13728 (2021). DOI: 10.1038/s41598-021-93011-3
[8] A.A. Andreev, R. Sonobe, S. Kawata, S. Miyazaki, K. Sakai, K. Miyauchi, T. Kikuchi, K. Platonov, K. Nemoto. Plasma Phys. Control. Fusion, **48**, 1605 (2006). DOI: 10.1088/0741-3335/48/11/003
[9] J. Fuchs, C.A. Cecchetti, M. Borghesi, T. Grismayer, E. d'Humiéres, P. Antici, S. Atzeni, P. Mora, A. Pipahl, L. Romagnani, A. Schiavi, Y. Sentoku, T. Toncian, P. Audebert, O. Willi. Phys. Rev. Lett., **99** (1), 015002 (2007). DOI: 10.1103/PhysRevLett.99.015002
[10] S.I. Glazyrin, A.V. Brantov, M.A. Rakitina, V.Yu. Bychenkov. High Energy Density Phys., **36**, 100824 (2020). DOI: 10.1016/j.hedp.2020.100824
[11] D. Batani, R. Jafer, M. Veltcheva, R. Dezulian, O. Lundh, F. Lindau, A. Persson, K. Osvay, C.-G. Wahlström, D.C. Carroll, P. McKenna, A. Flacco, V. Malka. New J. Phys., **12**, 045018 (2010). DOI: 10.1088/1367-2630/12/4/045018

Translated by Y.Deineka